BNL-226012-2024-JAAM

Chalcogen effect on the photovoltaic performance of nonfused-ring small molecular electron acceptors for efficient organic solar cells

S. Liu, R. Li

To be published in "Chemical Engineering Journal"

May 2024

Photon Sciences

Brookhaven National Laboratory

U.S. Department of Energy

USDOE Office of Science (SC), Basic Energy Sciences (BES)

Notice: This manuscript has been authored by employees of Brookhaven Science Associates, LLC under Contract No.DE-SC0012704 with the U.S. Department of Energy. The publisher by accepting the manuscript for publication acknowledges that the United States Government retains a non-exclusive, paid-up, irrevocable, world-wide license to publish or reproduce the published form of this manuscript, or allow others to do so, for United States Government purposes.

DISCLAIMER

This report was prepared as an account of work sponsored by an agency of the United States Government. Neither the United States Government nor any agency thereof, nor any of their employees, nor any of their contractors, subcontractors, or their employees, makes any warranty, express or implied, or assumes any legal liability or responsibility for the accuracy, completeness, or any third party's use or the results of such use of any information, apparatus, product, or process disclosed, or represents that its use would not infringe privately owned rights. Reference herein to any specific commercial product, process, or service by trade name, trademark, manufacturer, or otherwise, does not necessarily constitute or imply its endorsement, recommendation, or favoring by the United States Government or any agency thereof or its contractors or subcontractors. The views and opinions of authors expressed herein do not necessarily state or reflect those of the United States Government or any agency thereof.

Chalcogen Effect on the Photovoltaic Performance of Nonfused-Ring Small Molecular Electron Acceptors for Efficient Organic Solar Cells

Siyang Liu,[a] Xiaowei Chen,[a] Yinfeng Li,[a] Xiaopeng Xu,[a,*] Liyang Yu,[a] Yuwei Duan,[b] Ruipeng Li,[c] Qiang Peng[a,b,*]

[a] School of Chemical Engineering and State Key Laboratory of Polymer Materials Engineering, Sichuan University, Chengdu 610065, P. R. China.

[b] College of Materials and Chemistry & Chemical Engineering, Chengdu University of Technology, Chengdu 610059, P. R. China.

[c] National Synchrotron Light Source II Brookhaven National Lab, Suffolk, Upton, NY 11973, USA

*To whom correspondence should be addressed: Tel: +86-28-85415506; fax: +86-28-85415506; email: xpxu@scu.edu.cn; qiangpeng@scu.edu.cn

Abstract

Fused-ring electron acceptors (FREAs) are the current working horse for the top performing organic solar cells (OSCs). Nevertheless, these FREAs surfer from high synthetic complexity, production costs and poor scalability, hindering their industrialization. Developing nonfused-ring electron acceptors (NFREAs) is a more feasible alternative solution towards future photovoltaic applications. In this work, a series of NFREAs have been designed and synthesized by introducing chalcogen atoms on the side chains for OSCs. The introduced chalcogen atoms (O, S, and Se) not only modulated the energy levels but also finely tuned the intermolecular interactions. Especially, the formed S···S and Se···Se intermolecular interactions in TTS-4F and TTSe-4F resulted in higher molecular crystallinity than TTO-4F. Unexpectedly, the strong Se···Se interactions also led the aggregation of TTSe-4F and formation of large domains in the PM6:TTSe-4F blend. The moderate S···S interactions in TTS-4F enabled an optimal phase separation with more ideal nano fibrils distributed in the PM6:TTS-4F blend, facilitating the charge separation and transport. As a result, TTS-4F based devices achieved a champion power conversion efficiency (PCE) of 14.74%, higher than the TTO-4F (8.76%) and TTSe-4F (11.56%) based devices.

Keywords: organic solar cells, nonfused-ring electron acceptors, side chain engineering, chalcogen atom substitution; power conversion efficiency

1. Introduction

Organic solar cells (OSCs) are promising next generation renewable low-carbon energy technology, owing to their unique merits of wide raw material sources, ease of mass production by solution processing, light-weight for portable electronics, and mechanical flexibility for wearable devices.[1-3] Thanking to the great success of fused-ring electron acceptors (FREAs) with improved near-infrared (NIR) light-harvesting properties and readily-tunable molecular orbital energy levels, the power conversion efficiency (PCE) of OSCs has skyrocketed from around 10% to more than 19% in the past ten years.[4-9] Despite fused-ring cores with π-extended backbones play a critical role in achieving excellent photovoltaic performance, the multiple-step ring-fusing reactions make them suffer from synthetic complexity, high production costs and poor scalability, hindering their industrialization.[10-13] Therefore, it still a great need to develop efficient small molecular acceptors with more simple structures and easy synthesis towards the future applications.

To conquer the disadvantages associated with FREAs, nonfused-ring electron acceptors (NFREAs) have been proposed.[13-15] By replacing fused-ring cores in FREAs with nonfused-ring skeletons, NFREAs possess greater synthetic flexibility with fewer synthetic steps and higher yields.[13, 16] However, the NFREAs with C–C single bonds connecting adjacent building blocks lead to rotatable conformation and poor molecular planarity for ordered molecular packing.[17] To mediate the molecular planarity, a successful strategy is introducing intramolecular noncovalent interactions by heteroatoms (such as O···S, N···S, F···S, F···H, and O···H noncovalent bonds).[11, 13, 18-26] These noncovalent interactions serve as confirmation locks restricting the rotation to improve the coplanar structure and electron transport of NFREAs. In

addition to the noncovalent interactions, Hou *et al* proposed a strategy of introducing large steric hindrance to develop NFREAs, which endowed them with good planarity, high conformational stability and favorable molecular packing mode.[27-30] Most recently, Song *et al* encapsulated the tetrathiophene core with macrocyclic ring, which restricted the *cis*- and twisted conformation of the resultant NFREA to generate a more conformational stable and planar molecular backbone.[31] With the rational combination of above design strategies, the PCEs of NFREAs were successfully boosted up to 15-17%,[12, 27, 31-36] which are almost on par with FREAs.

As above mentioned, the molecular confirmation plays a key role in affecting the molecular packing order and the performance of NFREAs. With regards to introducing intramolecular noncovalent interactions in the NFREAs, the alkoxy side chains containing the O atoms have been extensively applied, which enabled the introduction of O···S and O···H noncovalent interactions.[26, 37-47] Nevertheless, other chalcogen atoms are poorly studied.[48, 49] Even in the FREAs, only limited reports employed alkylthio side chains to develop efficient acceptors *via* introducing O···S, S···S interactions.[50-53] Among them, some studies showed that the alkylthio side chains containing S atoms used in the FREAs outperformed the alkoxy side chains,[50-52] while still other examples showed the opposite tendency.[53] In the case of NFREAs, their applications remain to be better understood. In addition, many acceptor materials based on selenophene ring containing the Se atom have been reported and showed excellent performances.[54-56] Se has much richer, larger and more easily polarized electron clouds and intermolecular Se···Se interactions compared to S.[54, 57] The more electron rich and polarizable nature also enhances the quinoidal character of corresponding materials, resulting in redshifted

absorption.[54] However, alkylseleno side chains containing Se atom has never been used to develop donor and acceptor materials, and their application potential remains to be disclosed.

In this work, we report a series of new NFREAs by introducing chalcogen atoms (O, S, and Se) on the side chains for high performance OSCs (Scheme 1). In these NFREAs, thieno[3,2-b]thiophene (TT) was used as the main electron donating block, 2,4,6-triisopropylphenyl (TIP) was attached to the TT block to serve as the steric hindrance substituent, outward 2-ethylhexyloxy, 2-ethylhexylthio and 2-ethylhexylseleno side chains (with O, S, and Se substitution, respectively) were introduced into the bilateral thiophene units, and fluorinated cyanoindone was used as the electron-withdrawing terminal. The effect of chalcogen atoms on the overall photovoltaic property was systematically investigated. Among three NRFEAs, the moderate S···S interactions in TTS-4F molecules guaranteed the high crystallinity and enabled an optimal blend morphology, facilitating the charge separation and transport. As a result, TTS-4F based devices achieved a champion PCE of 14.74%, higher than the TTO-4F (8.76%) and TTSe-4F (11.56%) based devices.

2. Results and discussion

2.1. Materials synthesis and characterization

Scheme 1b shows the synthetic routes of the NFREAs. The alkylation of compound 1 followed by bromination afforded compound 4. Compound 4 was lithiated and followed by reaction with trimethyl silicon chloride and tributyl tin chloride afforded compound 6 successfully. The Stille-coupling of compound 7 with compounds 8, 9 and 6, respectively, produced compounds 10a, 10b and 10c. The final NRFEAs of TTO-4F, TTS-4F and TTSe-4F were obtained by Knoevenagel condensation of compound 11 with compounds 10a, 10b and 10c, respectively.

The detailed synthetic procedures and chemical verification were presented in Supporting Information (SI). All the acceptors exhibited decent thermal stability with a decomposition temperature (T_d, 5% weight loss) of 281 °C for TTO-4F, 311 °C for TTS-4F and 213 °C for TTSe-4F, respectively, as determined by the thermogravimetric analysis (TGA, Fig. S1a). In the differential scanning calorimetry (DSC) curves, TTS-4F showed an obvious endothermic transition with a melting peak of 118 °C (Fig. S1b).

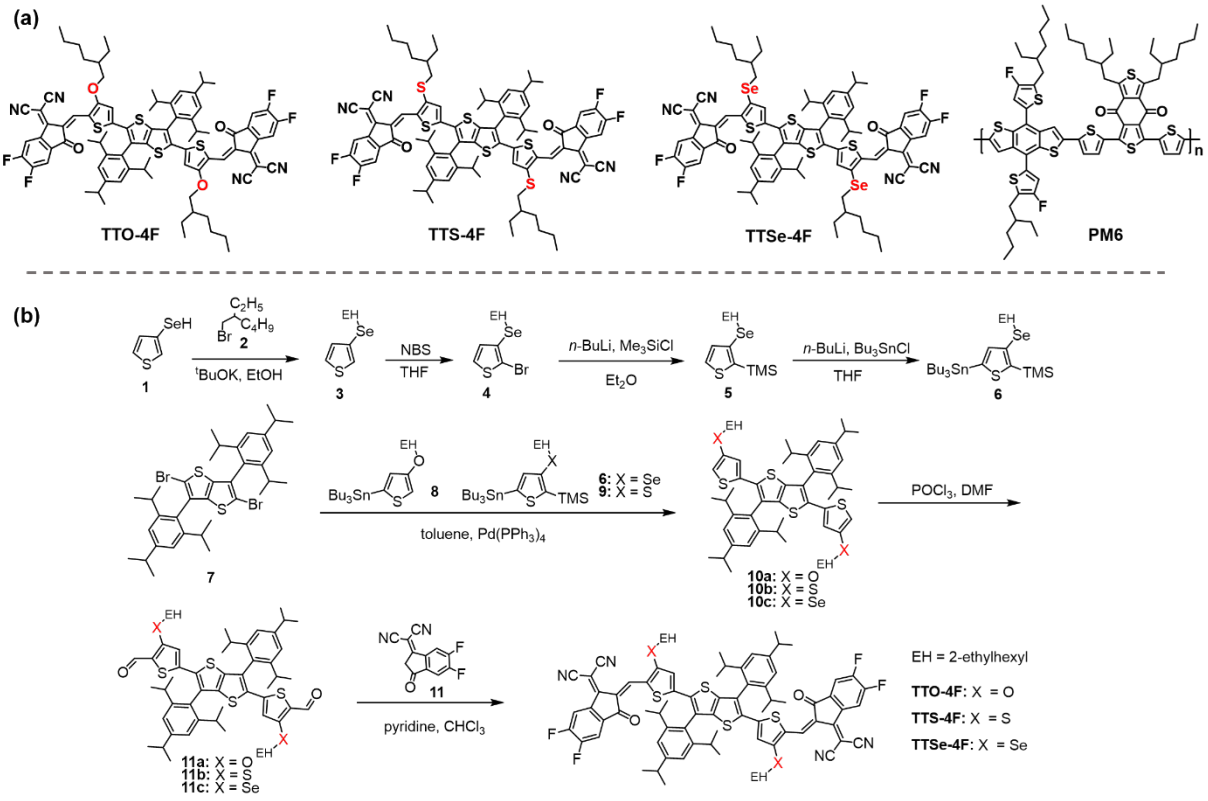

Scheme 1. (a) The chemical structures of the NFREAs and PM6 donor. (b) The synthetic routes of the NFREAs.

2.2. Optical properties and energy levels

These NFREAs showed very similar absorption profiles with an intense absorption strength 600-750 nm in diluted chloroform solution (Fig. 1a). The maximum molar extinction coefficients (ε) were 1.55×10^5 M^{-1} cm^{-1} for TTO-4F (at 708 nm), 1.53×10^5 M^{-1} cm^{-1} for TTS-

4F (at 702 nm) and 1.52×10^5 M^{-1} cm^{-1} for TTSe-4F (at 701 nm), respectively (Table 1). The slightly redshifted absorption peak with higher absorption strength of TTO-4F was due to the outer alkoxy side chains inducing smaller steric hindrance in solution. Nevertheless, TTS-4F and TTSe-4F showed more redshifted in film state than TTO-4F (Fig. 1b). The optical bandgaps (E_g^{opt}) were estimated to be 1.55, 1.54 and 1.53 eV for TTO-4F, TTS-4F and TTSe-4F, respectively. The results indicated that the TTS-4F and TTSe-4F thin films possessed the more ordered molecular packing induced by the intermolecular S···S and Se···Se interactions, respectively. The NFREAs also exhibited well complementary absorptions with the PM6 donor.

The energy levels of the NFREAs were studied by cyclic voltammetry (CV) experiments (Fig. 1c,d and Table 1). The onset oxidation potentials were 1.40, 1.44 and 1.42 V for TTO-4F, TTS-4F and TTSe-4F, corresponding to their highest occupied molecular orbital (HOMO) energy levels of -5.77, -5.81 and -5.79 eV, respectively. The onset reduction potentials were -0.48, -0.42 and -0.42 V for TTO-4F, TTS-4F and TTSe-4F, corresponding to their lowest unoccupied molecular orbital (LUMO) energy levels of -3.89, -3.95 and -3.95 eV, respectively. The higher HOMO and LUMO energy levels of TTO-4F were ascribed to the more electron donating effect of alkoxy side chains, which indicated that the TTO-4F device would obtain higher open-circuit voltage (V_{oc}).

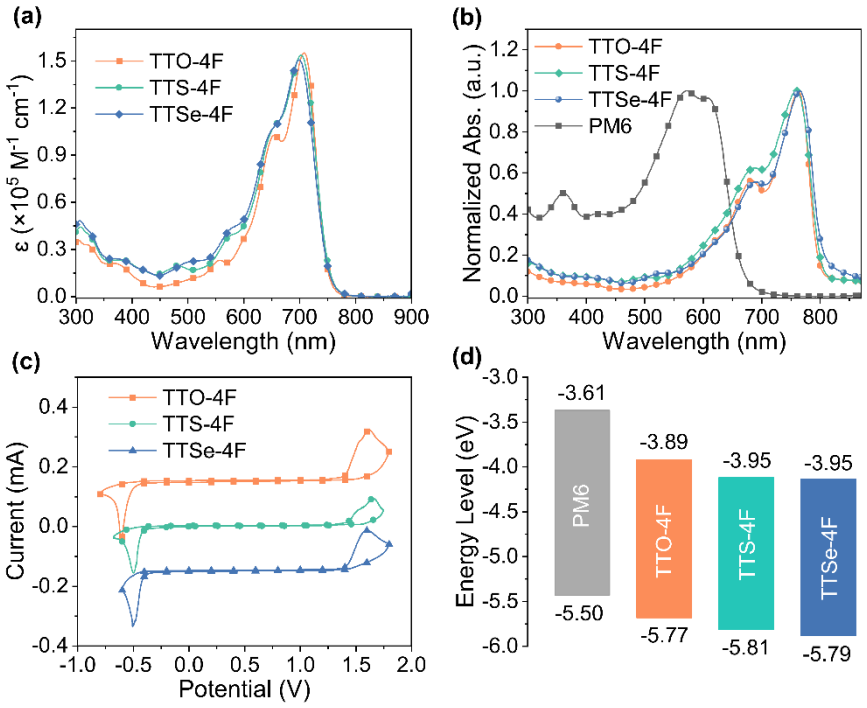

Fig. 1. (a) Molar extinction coefficient profiles of the NFREAs. (b) Normalized absorption spectra of the donor and acceptors. (c) CV curves of the NFREAs. (d) Energy level diagram of the donor and acceptors.

Table 1. Optical and electrochemical parameters of the NFREAs.

Acceptor	λ_{peak}^{sol} (nm)	ε (M^{-1} cm^{-1})	λ_{peak}^{film} (nm)	E_g^{opt} (eV)	HOMO (eV)	HOMO (eV)	E_g^{CV} (eV)
TTO-4F	708	1.55×10^5	683,762	1.55	-5.77	-3.89	1.88
TTS-4F	702	1.53×10^5	687,759	1.54	-5.81	-3.95	1.86
TTSe-4F	701	1.52×10^5	690,765	1.53	-5.79	-3.95	1.84

The chalcogen substitution effect on the molecular geometry and electronic properties was studied by density functional theory (DFT) at the B3LYP/6-31G (d, p) basis set (Fig. 2). All three NFREAs exhibited comparable torsional energies between the TT block and the steric TIP side chains (Fig. 2a). Besides, they exhibited closed torsional energies between the TT block and the chalcogen substituted thiophene bridges (Fig. 2b). In contrast, torsional energy between the chalcogen substituted thiophene bridge and the terminal group was slightly increased from

TTO-4F to TTS-4F and TTSe-4F (Fig. 2c). The results indicated that the outer chalcogen substituted alkyl chains had more profound effect on the rotation of the end groups. In addition, compared to the other two side chains, the alkoxy side chains led to more positive local electrostatic potential (ESP) of TTO-4F (Fig. 2d), thus influencing the charge distribution. The HOMO/LUMO levels were -5.60/-3.47, -5.71/3.60 and -5.69/-3.61 eV for TTO-4F, TTS-4F and TTSe-4F, respectively, which were similar to the variation trends obtained from the CV measurements.

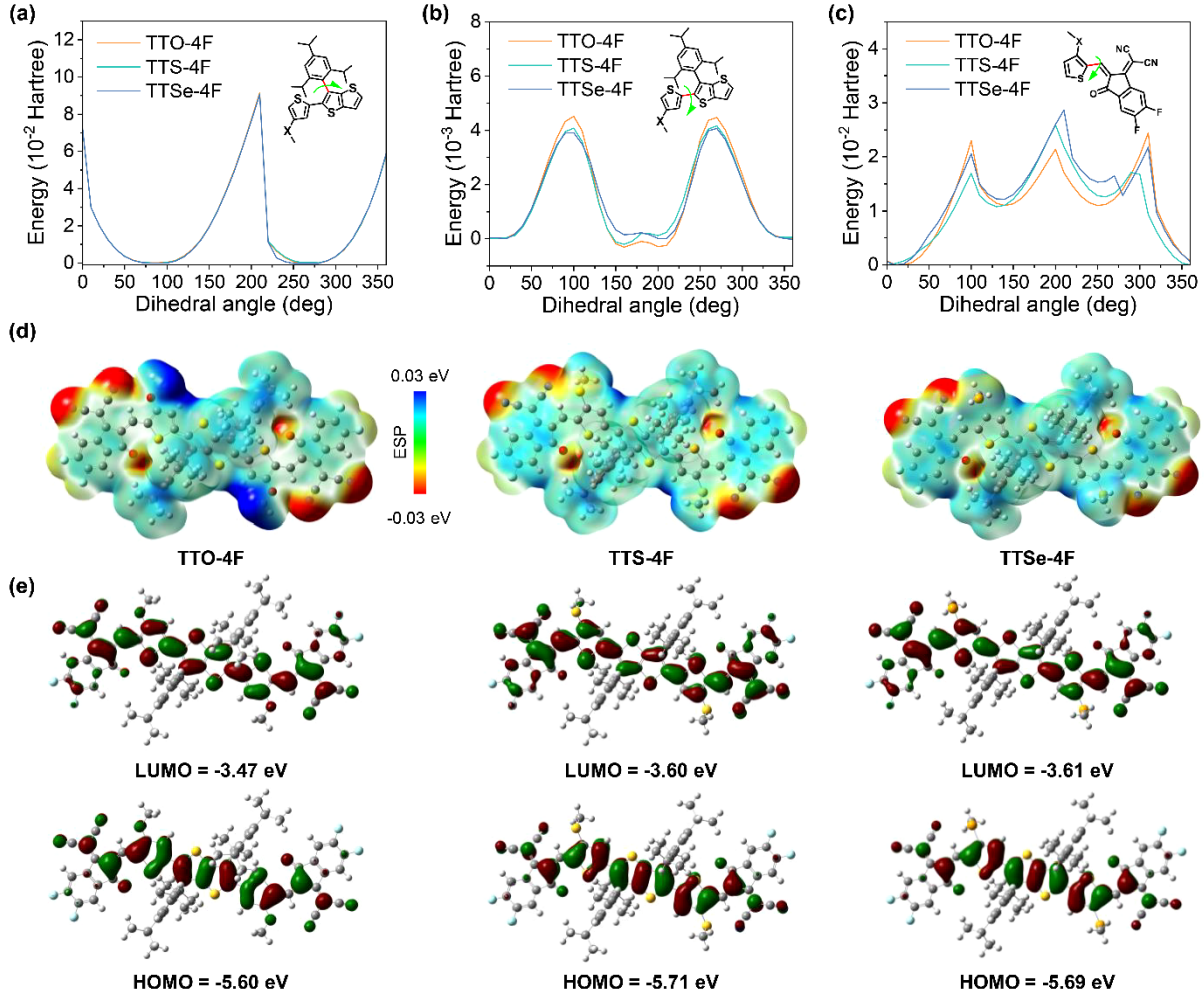

Fig. 2. (a-c) Torsional energy barriers between different units in the acceptors. (d) ESP distributions and (e) frontier molecular orbitals for simplified models of the acceptors.

2.3. Photovoltaic performances

The application potential of these NFREAs in OSCs was investigated by fabricating the devices based on a structure of indium tin oxide (ITO)/poly(3,4-ethylenedioxythiophene): poly(styrenesulfonate) (PEDOT:PSS)/PM6:NFREA/PNDIT-F3N/Ag (see device processing details in SI). The TTO-4F based devices obtained the highest V_{oc} of 0.954 V because of the smallest LUMO level offset between the donor and acceptor. However, the much lower short-circuit current density (J_{sc}) of 17.85 mA cm^{-2} and fill factor (FF) of 51.43% limited the PCE of TTO-4F based devices to 8.76% (Fig. 3 and Table 2). Although TTS-4F based devices exhibited a decreased V_{oc} of 0.907 V, the notably increased J_{sc} of 21.70 mA cm^{-2} and FF of 74.90% contributed to the largely improved PCE of 14.74%. TTSe-4F showed a further decreased V_{oc} of 0.905 V, a moderate J_{sc} of 20.54 mA cm^{-2} and an FF of 62.14%, delivering a decent PCE of 11.56%. The side chain engineering effect on the device performances was further studied by external quantum efficiency (EQE) measurements (Fig. 3b). TTS-4F and TTSe-4F based devices showed higher EQE responses over all the absorption range than the TTO-4F based devices, indicating their more efficient charge generation or extraction under illumination.

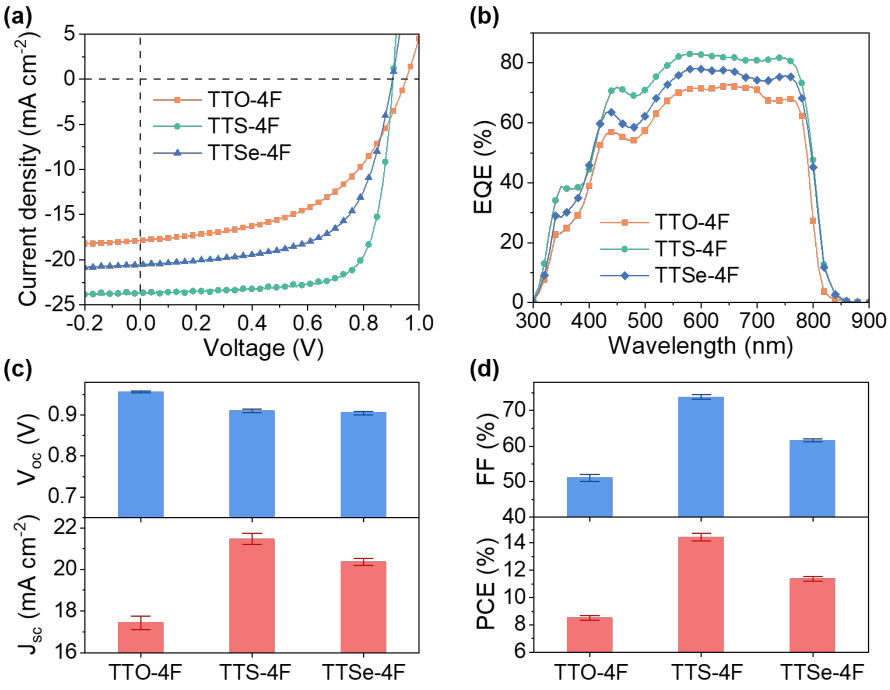

Fig. 3. (a) *J-V* curves and (b) EQE curves of the OSCs based on PM6 donor and the NFREAs. Column plots of (c) V_{oc} and J_{sc} and (d) FF and PCE distributions of the OSCs based on the PM6 donor and NFREAs.

Table 2. Photovoltaic parameters of the OSCs based on the PM6 donor and various acceptors.

Acceptor	V_{oc} (V)	J_{sc} (mA cm^{-2})	J_{EQE}[b] (mA cm^{-2})	FF (%)	PCE (%)
TTO-4F	0.954 (0.956±0.002)[a]	17.85 (17.44±0.33)	17.44	51.43 (51.04±0.99]	8.76 (8.51±0.17)
TTS-4F	0.907 (0.910±0.005)	21.70 (21.46±0.27)	21.25	74.90 (73.82±0.65]	14.74 (14.43±0.27)
TTSe-4F	0.905 (0.905±0.004)	20.54 (20.36±0.17)	19.76	62.14 (61.62±0.40]	11.56 (11.36±0.17)

[a] The averaged values with standard deviations in the parentheses were calculated from 20 individual devices; [b] The integrated current densities were calculated from the EQE curves.

2.4. Molecular packing behaviors and charge transport properties

The molecular packing behaviors of the pristine NFREA films and blend films were studied by

grazing incidence wide-angle X-ray scattering (GIWAXS) measurements (Fig. 4 and Table S1). The pristine films of TTO-4F and TTS-4F showed a typical edge-on packing, with a lamellar stacking in the out-of-plane direction while a π-π stacking in the in-plane direction. In contrast, a spotted diffraction was observed from TTSe-4F film, which was due to its strong aggregation in film state. The lamellar packing distance (d_l) was reduced from 2.01 nm (q_z = 3.12 nm^{-1}) for TTO-4F, to 1.73 nm (q_z = 3.61 nm^{-1}) for TTS-4F, and 1.40 nm (q_z = 4.49 nm^{-1}) for TTSe-4F, respectively (Table S1). Moreover, the crystal coherence length (CCL) for the lamellar stacking was increased from 22.9 nm for TTO-4F, to 24.1 nm for TTS-4F, and 25.2 nm for TTSe-4F, respectively. The π-π stacking distance (d_π) was 0.343 nm (q_{xy} = 18.3 nm^{-1}) for TTO-4F and 0.345 nm (q_{xy} = 18.2 nm^{-1}) for TTS-4F, respectively. While the π-π stacking of TTSe-4F was difficulted to determine from the spotted GIWAXS image. Interestingly, TTO-4F and TTS-4F transfers from edge-on configuration to face-on when blend with the donor polymer. These were possibly due to their good miscibility with the polymer donor and the reduced aggregation in the blend films. Nevertheless, TTSe-4F lost the configurational anisotropy when blend with the PM6 donor, due to its strong aggregation and poor miscibility with PM6. The improved crystallinity of the blend films from PM6:TTO-4F to PM6:TTS-4F and PM6:TTSe-4F was also confirmed by the CCL values. In addition, PM6:TTSe-4F displayed multi-semicircle diffractions, which was due to the isotopically distributed aggregates of TTSe-4F in the blend film.

Space charge limited current (SCLC) measurements were performed to study the charge transport properties of the blend films (Fig. S2). The hole/electron mobilities (μ_h/μ_e) were estimated to be $1.31\times10^{-4}/7.20\times10^{-5}$, $2.76\times10^{-4}/2.31\times10^{-4}$ and $1.84\times10^{-4}/1.35\times10^{-4}$, $cm^2\ V^{-1}\ s^{-1}$

for TTO-4F, TTS-4F and TTSe-4F based blends, respectively. The higher μ_h and μ_e values of TTS-4F based blend were originated from the more ordered molecular packing observed from the GIWAXS measurements, which were conducive to reducing charge recombination in devices.

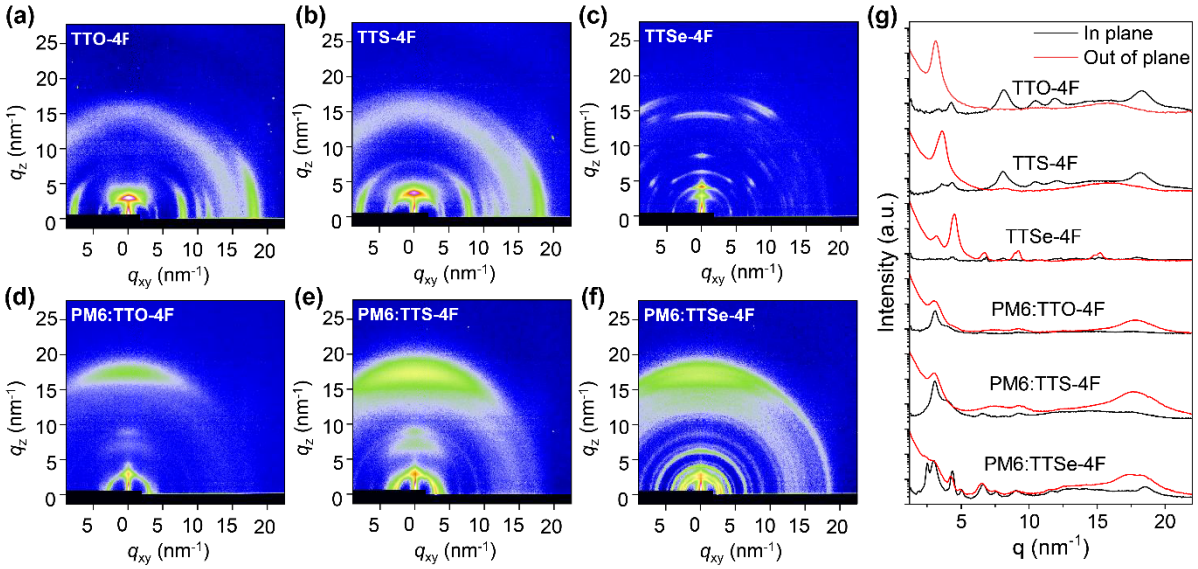

Fig. 4. (a-f) GIWAXS patterns of the pristine and blend films. (g) The in-plane and out-of-plane line-cuts from the GIWAXS patterns.

2.5. Morphology studies

The chalcogen substitution effect on the blend morphology was investigated by atomic force microscopy (AFM) measurements (Fig. 5). All three blend films exhibited fibrillar networks resulted from the phase separation between donor and acceptors. Nevertheless, PM6:TTO-4F exhibited a quite rough surface with a large root mean-square (RMS) roughness (R_q) of 5.47 nm, which could lead to poor interfacial contact for charge extraction. In addition, as observed from the tapping phase image, the fibril widths were about 50 nm, much larger than the ideal domain size. This would increase the exciton diffusion barriers and decrease the charge dissociation efficiency in the corresponding devices. PM6:TTS-4F had a more smooth top

surface with a small RMS of 1.67 nm. Importantly, a well distributed nanofibril network with the fibril width about 18 nm could be observed from the tapping phase image. Such an optimal morphology was beneficial for both charge separation and transport, thus enabling higher device performance of the PM6:TTS-4F based devices. Although PM6:TTSe-4F have a relatively smooth top surface with a moderate RMS of 2.34 nm, TTSe-4F aggregated readily into large domains and separated from the network of PM6 fibrils. The aggregation of TTSe-4F was further confirmed by the optical microscope images of the pristine acceptor films (Fig. S3). Compared to the more uniform images of TTO-4F and TTS-4F films, large crystals could be observed in the image of TTSe-4F film. The aggregation of TTSe-4F in the blend film resulted in uneven distribution of TTSe-4F and the reduced absorption in the longer wavelength range (Fig. S4). This was also detrimental to the charge separation in devices, thus lowering the photovoltaic performances.

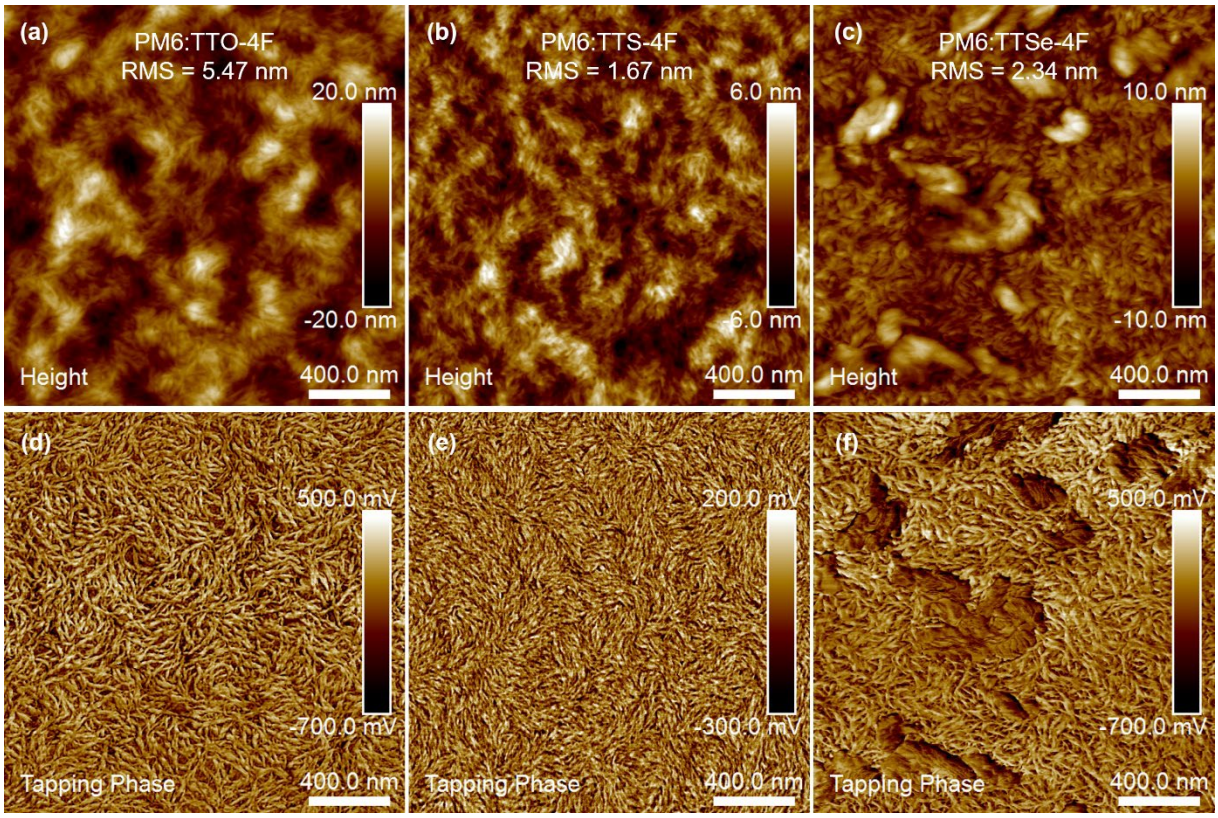

Fig. 5. AFM (a-c) height images and (d-f) phase images of the blend films.

2.6. Charge generation and recombination dynamics

The chalcogen substitution effect on the charge generation kinetics was studied by femtosecond transient absorption spectroscopy (fs-TAS) measurements (Fig. 6). An excitation wavelength of 720 nm was chosen to excite the NFREAs to study the hole transfer from the acceptors to the donor. The ground-state bleach (GSB) signals around 600 and 800 nm belonged to PM6 donor and the NFREAs, respectively. TTS-4F and TTSe-4F based blends showed much stronger GSB signals around 600 nm, indicating their more efficient hole transfer than TTO-4F based blend. The charge transfer lifetimes were quantified by fitting the GSB signals of PM6 donor at 630 nm *via* a biexponential function, where component τ_1 was assigned to the ultrafast interfacial hole-transfer process and the second component τ_2 represented the diffusion-limited dissociation of bulk excitons.[2] The τ_1/τ_2 were estimated to be 1.62/16.7 ps for PM6:TTO-4F, 0.43/9.2 ps for PM6:TTS-4F and 1.21/12.5 ps for PM6:TTSe-4F, respectively. The smaller τ_1/τ_2 of PM6:TTS-4F blend indicated the faster hole transfer in the corresponding devices.

Transient photocurrent (TPC) measurements were performed to study the charge extraction information of the devices (Fig. 6e). The charge extraction times of the devices were calculated to be 0.28, 0.24 and 0.25 μs for TTO-4F, TTS-4F and TTSe-4F based devices, respectively. On the other hand, transient photovoltage (TPV) measurements were conducted to investigate the charge recombination in the devices (Fig. 6f). The charge lifetimes calculated from the fitted TPV kinetics were 12.1, 15.3 and 13.6 μs for TTO-4F, TTS-4F and TTSe-4F based devices, respectively. The longer charge lifetime and shorter charge extraction time in TTS-4F based devices could contributed to the more efficient charge extraction and reduced charge

recombination, thus resulting in the higher device performances.

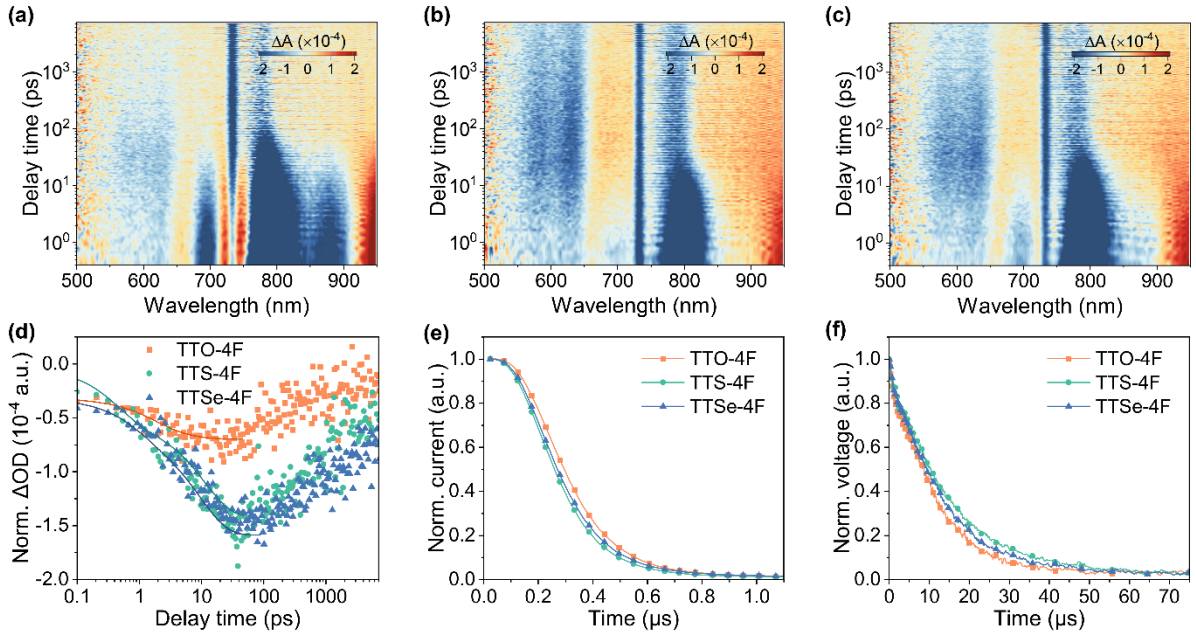

Fig. 6. fs-TAS images of (a) PM6:TTO-4F, (b) PM6:TTS-4F and (c) PM6:TTSe-4F films. (d) fs-TAS kinetics of the blend films (pumped at 720 nm, probed at 630 nm). (e) Normalized TPC of the devices. (f) Normalized TPV of the devices.

3. Conclusion

In summary, we designed and synthesized a series of NFREAs, namely TTO-4F, TTS-4F and TTSe-4F, by introducing chalcogen atoms on the side chains. In these NFREAs, the TIP substituted TT central core enabled the conformational stability for favorable molecular packing. The outward side chains with chalcogen atom substitutions on the thiophene bridges not only modulated the energy levels but also finely tuned the molecular packing behavior and blend morphology. The TTS-4F and TTSe-4F based blends exhibited higher crystallinity than the TTO-4F based blend, which was due to the intermolecular S···S interactions between TTS-4F molecules and Se···Se interactions between TTSe-4F molecules. But unexpectedly, the strong Se···Se interactions induced the aggregation of TTSe-4F to form large domains in

PM6:TTSe-4F blend, which were detrimental to the charge separation in devices. In contrast, The more suitable S···S interactions in TTS-4F made the PM6:TTS-4F blend form more uniform nanofibril networks with suitable size of nanofibrils, facilizing the charge separation and transport. As a result, the TTS-4F based devices achieved a champion PCE of 14.74%, much higher than TTO-4F (8.76%) and TTSe-4F (11.56%) based devices. This work highlighted the importance of side chain engineering and chalcogen effect for developing highly efficient NFREAs.

Declaration of Competing Interest

The authors declare that they have no known competing financial interests or personal relationships that could have appeared to influence the work reported in this paper.

Data availability

Data will be made available on request.

Acknowledgements

This work was financially supported by the National Key Research and Development Program of China (Grant No. 2022YFB4200500), National Natural Science Foundation of China (NSFC, 21825502, 22075190, 22379101, 21905185 and 22105135), Sichuan Natural Science Foundation (2023NSFSC0304), the School Local Science and Technology Cooperation Special Funds of Sichuan University and Zigong City (2020CDZG-6), Special Fund for Strategic Cooperation Between Sichuan University and Yibin Municipal People's Government (2020CDYB-28), Special Fund for Strategic Cooperation Between Sichuan University and Suining City (2022CDSN-01), Special Fund for Strategic Cooperation Between Sichuan University and Dazhou City (2022CDDZ-04), and the Fundamental Research Funds for the

Central Universities (YJ201957, YJ202069 and YJ202116). The authors thank Yanping Huang from Center of Engineering Experimental Teaching, School of Chemical Engineering, Sichuan University for the help of NMR measurements and National Synchrotron Light Source II (NSLS-II, Contract No. DE-SC0012704) Brookhaven National Laboratory for providing GIWAXS experiment time.

Appendix A. Supplementary data

Supplementary data to this article can be found online at XXX

References

[1] J. Yi, G. Zhang, H. Yu, H. Yan. Advantages, challenges and molecular design of different material types used in organic solar cells. Nat. Rev. Mater. 9 (2024) 46-62, https://doi.org/10.1038/s41578-023-00618-1.

[2] P. Wu, Y. Duan, Y. Li, X. Xu, R. Li, L. Yu, Q. Peng. 18.6% efficiency all-polymer solar cells enabled by a wide bandgap polymer donor based on benzo[1,2-d:4,5-d′]bisthiazole. Adv. Mater. 36 (2024) 2306990, https://doi.org/10.1002/adma.202306990.

[3] H. Zhuo, X. Li, J. Zhang, C. Zhu, H. He, K. Ding, J. Li, L. Meng, H. Ade, Y. Li. Precise synthesis and photovoltaic properties of giant molecule acceptors. Nat. Commun. 14 (2023) 7996, https://doi.org/10.1038/s41467-023-43846-3.

[4] W. Liu, H. Zhang, S. Liang, T. Wang, S. He, Y. Hu, R. Zhang, H. Ning, J. Ren, A. Bakulin, F. Gao, J. Yuan, Y. Zou. The synthesis of a multiple d-a conjugated macrocycle and its application in organic photovoltaic. Angew. Chem. Int. Ed. 62 (2023) e202311645, https://doi.org/10.1002/anie.202311645.

[5] X. Xu, W. Jing, H. Meng, Y. Guo, L. Yu, R. Li, Q. Peng. Sequential deposition of multicomponent bulk heterojunctions increases efficiency of organic solar cells. Adv. Mater. 35 (2023) 2208997, https://doi.org/10.1002/adma.202208997.

[6] Y.Z. Lin, J.Y. Wang, Z.G. Zhang, H.T. Bai, Y.F. Li, D.B. Zhu, X.W. Zhan. An electron acceptor challenging fullerenes for efficient polymer solar cells. Adv. Mater. 27 (2015) 1170-1174, https://doi.org/10.1002/adma.201404317.

[7] J. Yuan, Y.Q. Zhang, L.Y. Zhou, G.C. Zhang, H.L. Yip, T.K. Lau, X.H. Lu, C. Zhu, H.J. Peng, P.A. Johnson, M. Leclerc, Y. Cao, J. Ulanski, Y.F. Li, Y.P. Zou. Single-junction organic solar cell with over 15% efficiency using fused-ring acceptor with electron-deficient core. Joule 3 (2019) 1140-1151, https://doi.org/10.1016/j.joule.2019.01.004.

[8] C. Li, J. Zhou, J. Song, J. Xu, H. Zhang, X. Zhang, J. Guo, L. Zhu, D. Wei, G. Han, J. Min, Y. Zhang, Z. Xie, Y. Yi, H. Yan, F. Gao, F. Liu, Y. Sun. Non-fullerene acceptors with branched side chains and improved molecular packing to exceed 18% efficiency in organic solar cells. Nat. Energy 6 (2021) 605-613, https://doi.org/10.1038/s41560-021-00820-x.

[9] L. Zhu, M. Zhang, J. Xu, C. Li, J. Yan, G. Zhou, W. Zhong, T. Hao, J. Song, X. Xue, Z. Zhou, R. Zeng, H. Zhu, C.C. Chen, R.C.I. MacKenzie, Y. Zou, J. Nelson, Y. Zhang, Y. Sun, F. Liu. Single-junction

organic solar cells with over 19% efficiency enabled by a refined double-fibril network morphology. Nat. Mater. 21 (2022) 656-663, https://doi.org/10.1038/s41563-022-01244-y.

[10] Q.Q. Bai, Q.M. Liang, H.N. Li, H.L. Sun, X.G. Guo, L. Niu. Recent progress in low-cost noncovalently fused-ring electron acceptors for organic solar cells. Aggregate 3 (2022) e281, https://doi.org/10.1002/agt2.281.

[11] T.J. Wen, Z.X. Liu, Z. Chen, J. Zhou, Z. Shen, Y. Xiao, X. Lu, Z. Xie, H. Zhu, C.Z. Li, H. Chen. Simple non-fused electron acceptors leading to efficient organic photovoltaics. Angew. Chem. Int. Ed. 60 (2021) 12964-12970, https://doi.org/10.1002/anie.202101867.

[12] D.L. Ma, Q.Q. Zhang, C.Z. Li. Unsymmetrically chlorinated non-fused electron acceptor leads to high-efficiency and stable organic solar cells. Angew. Chem. Int. Ed. 62 (2023) e202214931, https://doi.org/10.1002/anie.202214931.

[13] Z.P. Yu, Z.X. Liu, F.X. Chen, R. Qin, T.K. Lau, J.L. Yin, X.Q. Kong, X.H. Lu, M.M. Shi, C.Z. Li, H.Z. Chen. Simple non-fused electron acceptors for efficient and stable organic solar cells. Nat. Commun. 10 (2019) 2152, http://doi.org/10.1038/s41467-019-10098-z.

[14] Y. Xu, X. Gao, X. Song, D. You, J. Wang, J. Wang, Y. Wu, X. Tao, J. Ye, Y. Tao. Fully-unfused electron acceptors based on a steric boron dipyrromethene (bodipy) core for organic solar cells. New J. Chem. 47 (2023) 11792-11799, https://doi.org/10.1039/d3nj00845b.

[15] Y. Li, J. Yu, Y. Zhou, Z.a. Li. Molecular insights of non-fused ring acceptors for high-performance non-fullerene organic solar cells. Chem. Eur. J. 28 (2022) e202201675, https://doi.org/10.1002/chem.202201675.

[16] D. Luo, X. Lai, N. Zheng, C. Duan, Z. Wang, K. Wang, A.K.K. Kyaw. High-performance and low-energy loss organic solar cells with non-fused ring acceptor by alkyl chain engineering. Chem. Eng. J. 420 (2021) 129768, https://doi.org/10.1016/j.cej.2021.129768.

[17] M. Yang, W. Wei, X. Zhou, Z. Wang, C. Duan. Non-fused ring acceptors for organic solar cells. Energy Mater. 1 (2021) 100008, https://doi.org/10.20517/energymater.2021.08.

[18] J. Zhao, X. Xu, L. Yu, R. Li, Y. Li, Q. Peng. Highly efficient non-fused-ring electron acceptors enabled by the conformational lock and structural isomerization effects. ACS Appl. Mater. Interfaces 13 (2021) 25214-25223, http://dx.doi.org/10.1021/acsami.1c06299.

[19] X.-B. Gu, J.-H. Gao, Z.-Y. Han, Y.-H. Shi, Y.-N. Wei, Y.-C. Zhang, Q. Peng, Z.-X. Wei, X. Zhang, H. Huang. A simple building block with noncovalently conformational locks towards constructing low-cost and high-performance nonfused ring electron acceptors. Chin. J. Polym. Sci. 41 (2022) 556-563, https://doi.org/10.1007/s10118-022-2888-9.

[20] M. Li, S. Feng, S. Shen, H. Huang, W. Xue, N. Yu, Y. Zhou, W. Ma, J. Song, Z. Tang, Z. Bo. High efficiency ternary organic solar cells via morphology regulation with asymmetric nonfused ring electron acceptor. Chem. Eng. J. 438 (2022) 135384, https://doi.org/10.1016/j.cej.2022.135384.

[21] H. Lu, X. Wang, S. Li, D. Li, N. Yu, Z. Tang, Y. Liu, X. Xu, Z. Bo. Diphenylamine substituted high-performance fully nonfused ring electron acceptors: The effect of isomerism. Chem. Eng. J. 435 (2022) 134987, https://doi.org/10.1016/j.cej.2022.134987.

[22] X. Zheng, W. Liu, H. Lu, N. Yu, Y. Wang, H. Huang, S. Li, X. Wang, H. Wang, Y. Liu, X. Xu, Z. Tang, Z. Bo. A simple high-performance fully nonfused ring electron acceptor with a planar molecular backbone. Chem. Eng. J. 444 (2022) 136472, http://doi.org/10.1016/j.cej.2022.136472.

[23] A. Mishra, G.D. Sharma. Harnessing the structure-performance relationships in designing non-fused ring acceptors for organic solar cells. Angew. Chem. Int. Ed. 62 (2023) e202219245, https://doi.org/10.1002/anie.202219245.

[24] Q. Shen, C. He, B. Wu, Y. Lin, S. Chen, J. Gao, S. Li, Z. Ma, W. Ma, M. Shi, Y. Li, H. Chen. Progressive evolutions of non-fused ring electron acceptors toward efficient organic solar cells with improved photocurrent and reduced energy loss. Chem. Eng. J. 471 (2023) 144472, https://doi.org/10.1016/j.cej.2023.144472.

[25] J. Wang, Y. Wang, J. Li, Y. Yu, P. Bi, J. Qiao, Z. Chen, C. Wang, W. Wang, J. Dai, X. Hao, S. Zhang, J. Hou. Low-cost fully non-fused ring acceptor enables efficient organic photovoltaic modules for multi-scene applications. Angew. Chem. Int. Ed. (2023) e202314362, https://doi.org/10.1002/anie.202314362.

[26] Y.N. Chen, M. Li, Y. Wang, J. Wang, M. Zhang, Y. Zhou, J. Yang, Y. Liu, F. Liu, Z. Tang, Q. Bao, Z. Bo. A fully non-fused ring acceptor with planar backbone and near-ir absorption for high performance polymer solar cells. Angew. Chem. Int. Ed. 59 (2020) 22714-22720, https://doi.org/10.1002/anie.202010856.

[27] L. Ma, S. Zhang, J. Zhu, J. Wang, J. Ren, J. Zhang, J. Hou. Completely non-fused electron acceptor with 3d-interpenetrated crystalline structure enables efficient and stable organic solar cell. Nat. Commun. 12 (2021) 5093, https://doi.org/10.1038/s41467-021-25394-w.

[28] Y. Xiao, H. Yao, Y. Yang, C.E. Song, J. Wang, N. Yang, Z. Li, Y. Yu, D.H. Ryu, C. An, W.S. Shin, J. Hou. Selenium-based nonfused electron acceptors for efficient organic photovoltaic cells. Solar RRL 7 (2023) 2300095, https://doi.org/10.1002/solr.202300095.

[29] J. Li, H. Li, L. Ma, S. Zhang, J. Hou. Design and synthesis of n-alkylaniline-substituted low band-gap electron acceptors for photovoltaic application. Chin. J. Chem. 41 (2023) 424-430, https://doi.org/10.1002/cjoc.202200579.

[30] Z. Li, H. Yao, W. Wang, C.E. Song, D.H. Ryu, Y. Xiao, J. Wang, L. Ma, T. Zhang, J. Ren, C. An, W.S. Shin, J. Hou. Large steric hindrance enhanced molecular planarity for low-cost non-fused electron acceptors. ACS Appl. Mater. Interfaces 15 (2023) 16801-16808, https://doi.org/10.1021/acsami.3c01194.

[31] S. Shen, Y. Mi, Y. Ouyang, Y. Lin, J. Deng, W. Zhang, J. Zhang, Z. Ma, C. Zhang, J. Song, Z. Bo. Macrocyclic encapsulation in a non-fused tetrathiophene acceptor for efficient organic solar cells with high short-circuit current density. Angew. Chem. Int. Ed. (2023) e202316495, https://doi.org/10.1002/anie.202316495.

[32] L. Ma, S. Zhang, J. Ren, G. Wang, J. Li, Z. Chen, H. Yao, J. Hou. Design of a fully non-fused bulk heterojunction toward efficient and low-cost organic photovoltaics. Angew. Chem. Int. Ed. 62 (2023) e202214088, https://doi.org/10.1002/anie.202214088.

[33] S. Ye, C. He, Y. Pan, S. Li, S. Wang, C.-Z. Li, M. Shi, H. Chen. Regulating molecular packing and orientation of nonfused ring electron acceptors for organic solar cells with a high figure-of-merit. Solar RRL 7 (2023) 2300453, http://doi.org/10.1002/solr.202300453.

[34] X. Wang, R. Zeng, H. Lu, G. Ran, A. Zhang, Y.N. Chen, Y. Liu, F. Liu, W. Zhang, Z. Tang, Z. Bo. A simple nonfused ring electron acceptor with a power conversion efficiency over 16%†. Chin. J. Chem. 41 (2023) 665-671, https://doi.org/10.1002/cjoc.202200673.

[35] D. Li, H. Zhang, X. Cui, Y.N. Chen, N. Wei, G. Ran, H. Lu, S. Chen, W. Zhang, C. Li, Y. Liu, Y. Liu, Z. Bo. Halogenated nonfused ring electron acceptor for organic solar cells with a record efficiency of over 17%. Adv. Mater. (2023) 2310362, https://doi.org/10.1002/adma.202310362.

[36] X. Zheng, W. Liu, H. Wang, X. Man, G. Ran, X. Yu, H. Lu, Z. Bi, Y. Liu, A. Zhang, W. Ma, X. Xu, Z. Tang, W. Zhang, Z. Bo. Simple non-fused ring electron acceptors with well-controlled terminal group stacking. Cell Reports Physical Science 3 (2022) 101169, http://doi.org/10.1016/j.xcrp.2022.101169.

[37] X. Hu, Z. Qiao, D. Nodari, Q. He, J. Asatryan, M. Rimmele, Z. Chen, J. Martín, N. Gasparini, M.

Heeney. Remarkable isomer effect on the performance of fully non-fused non-fullerene acceptors in near-infrared organic photodetectors. Adv. Opt. Mater. (2023) 2302210, https://doi.org/10.1002/adom.202302210.

[38] H. Huang, Q. Guo, S. Feng, C.e. Zhang, Z. Bi, W. Xue, J. Yang, J. Song, C. Li, X. Xu, Z. Tang, W. Ma, Z. Bo. Noncovalently fused-ring electron acceptors with near-infrared absorption for high-performance organic solar cells. Nat. Commun. 10 (2019) 3038, https://doi.org/10.1038/s41467-019-11001-6.

[39] C. Wang, J. Fang, C. Guan, T. Wu, X. Liu, F. Liu, C. Xiao, W. Li. Non-fused polymerized small-molecule acceptors with a benzothiadiazole core for all-polymer solar cells. ACS Appl. Mater. Interfaces 15 (2023) 13363-13370, https://doi.org/10.1021/acsami.2c21574.

[40] X. Wang, H. Lu, A. Zhang, N. Yu, G. Ran, Z. Bi, X. Yu, X. Xu, Y. Liu, Z. Tang, W. Zhang, W. Ma, Z. Bo. Molecular-shape-controlled nonfused ring electron acceptors for high-performance organic solar cells with tunable phase morphology. ACS Appl. Mater. Interfaces 14 (2022) 28807-28815, https://doi.org/10.1021/acsami.2c04530.

[41] C. Li, X. Zhang, N. Yu, X. Gu, L. Qin, Y. Wei, X. Liu, J. Zhang, Z. Wei, Z. Tang, Q. Shi, H. Huang. Simple nonfused-ring electron acceptors with noncovalently conformational locks for low-cost and high-performance organic solar cells enabled by end-group engineering. Adv. Funct. Mater. 32 (2021) 2108861, https://doi.org/10.1002/adfm.202108861.

[42] X. Ding, X. Chen, Y. Xu, Z. Ni, T. He, H. Qiu, C.-Z. Li, Q. Zhang. A selenophene-containing near-infrared unfused acceptor for efficient organic solar cells. Chem. Eng. J. 429 (2022) 132298, https://doi.org/10.1016/j.cej.2021.132298.

[43] Y. Zhang, C. Zhang, A. Zhang, H. Wu, G. Ran, Y. Zhou, X. Wang, C. Li, Y. Liu, C. Yang, Z. Tang, W. Zhang, Z. Bo. Designing high-performance nonfused ring electron acceptors via synergistically adjusting side chains and electron-withdrawing end-groups. ACS Appl. Mater. Interfaces 14 (2022) 21287-21294, http://dx.doi.org/10.1021/acsami.2c01190.

[44] J. Cao, H. Wang, L. Yang, F. Du, J. Yu, W. Tang. Chlorinated unfused acceptor enabling 13.57% efficiency and 73.39% fill factor organic solar cells via fine-tuning alkoxyl chains on benzene core. Chem. Eng. J. 427 (2022) 131828, https://doi.org/10.1016/j.cej.2021.131828.

[45] J. Cao, S. Qu, L. Yang, H. Wang, F. Du, J. Yu, W. Tang. Asymmetric simple unfused acceptor enabling over 12% efficiency organic solar cells. Chem. Eng. J. 412 (2021) 128770, https://doi.org/10.1016/j.cej.2021.128770.

[46] Y. Liu, Z. Lin, J. Cao, F. Du, H. Wang, S. He, W. Tang. Unfused acceptors matching π-bridge blocks with proper frameworks enable over 12% as-cast organic solar cells. Small 18 (2022) 2201209, https://doi.org/10.1002/smll.202201209.

[47] Y. Chen, T. Liu, L.-K. Ma, W. Xue, R. Ma, J. Zhang, C. Ma, H.K. Kim, H. Yu, F. Bai, K.S. Wong, W. Ma, H. Yan, Y. Zou. Alkoxy substitution on idt-series and y-series non-fullerene acceptors yielding highly efficient organic solar cells. J. Mater. Chem. A 9 (2021) 7481-7490, https://doi.org/10.1039/d0ta10953c.

[48] W. Peng, G. Zhang, M. Zhu, H. Xia, Y. Zhang, H. Tan, Y. Liu, W. Chi, Q. Peng, W. Zhu. Simple-structured nir-absorbing small-molecule acceptors with a thiazolothiazole core: Multiple noncovalent conformational locks and d-a effect for efficient oscs. ACS Appl. Mater. Interfaces 11 (2019) 48128-48133, https://doi.org/10.1021/acsami.9b16686.

[49] Y. Xu, X. Chu, J. He, L. Huang, L. Dong, H. Qiu, Z. Ni, M. Li, Q. Zhang. Effect of alkylthio side chain isomerization of nonfused electron acceptors for organic solar cells. Dyes Pigments 219 (2023) 111563, https://doi.org/10.1016/j.dyepig.2023.111563.

[50] J. Chen, G. Li, Q. Zhu, X. Guo, Q. Fan, W. Ma, M. Zhang. Highly efficient near-infrared and semitransparent polymer solar cells based on an ultra-narrow bandgap nonfullerene acceptor. J. Mater. Chem. A 7 (2019) 3745-3751, https://doi.org/10.1039/c8ta11484f.

[51] L. Zhang, K. Jin, Z. Xiao, X. Wang, T. Wang, C. Yi, L. Ding. Alkoxythiophene and alkylthiothiophene π-bridges enhance the performance of a–d–a electron acceptors. Mater. Chem. Front. 3 (2019) 492-495, http://doi.org/10.1016/j.joule.2019.01.004.

[52] J. Hai, Y. Song, L. Li, X. Liu, X. Shi, Z. Huang, G. Qian, Z. Lu, J. Yu, H. Hu, S. Chen. High-efficiency organic solar cells enabled by chalcogen containing branched chain engineering: Balancing short-circuit current and open-circuit voltage, enhancing fill factor. Adv. Funct. Mater. 33 (2023) 2213429, https://doi.org/10.1002/adfm.202213429.

[53] Y.H. Liu, M. Li, J.J. Yang, W.Y. Xue, S.Y. Feng, J.S. Song, Z. Tang, W. Ma, Z.S. Bo. High-efficiency as-cast organic solar cells based on acceptors with steric hindrance induced planar terminal group. Adv. Energy Mater. 9 (2019) 1901280, https://doi.org/10.1002/aenm.201901280.

[54] B. Fan, F. Lin, X. Wu, Z. Zhu, A.K. Jen. Selenium-containing organic photovoltaic materials. Acc. Chem. Res. 54 (2021) 3906-3916, https://doi.org/10.1021/acs.accounts.1c00443.

[55] C. Yang, Q. An, H.R. Bai, H.F. Zhi, H.S. Ryu, A. Mahmood, X. Zhao, S. Zhang, H.Y. Woo, J.L. Wang. A synergistic strategy of manipulating the number of selenophene units and dissymmetric central core of small molecular acceptors enables polymer solar cells with 17.5 % efficiency. Angew. Chem. Int. Ed. 60 (2021) 19241-19252, https://doi.org/10.1002/anie.202104766.

[56] F. Qi, K. Jiang, F. Lin, Z. Wu, H. Zhang, W. Gao, Y. Li, Z. Cai, H.Y. Woo, Z. Zhu, A.K.Y. Jen. Over 17% efficiency binary organic solar cells with photoresponses reaching 1000 nm enabled by selenophene-fused nonfullerene acceptors. ACS Energy Lett. 6 (2021) 9-15, https://doi.org/10.1021/acsenergylett.0c02230.

[57] K. Liu, X. Xu, J. Wang, C. Zhang, G. Ge, F. Zhuang, H. Zhang, C. Yang, Q. Peng, J. Pei. Achieving high-performance non-halogenated nonfullerene acceptor-based organic solar cells with 13.7% efficiency via a synergistic strategy of an indacenodithieno[3,2-b]selenophene core unit and non-halogenated thiophene-based terminal group. J. Mater. Chem. A 7 (2019) 24389-24399, https://doi.org/10.1039/c9ta08328f.